Wireless Power Transmission Through Concrete Using Circuits Resonating at Utility Frequency of 60 Hz

Hiroki Ishida and Hiroto Furukawa

***Abstract*—A first attempt was made to perform wireless power transmission using circuits resonating at the utility frequency of 60 Hz. The purpose of this research is to develop a method for transmitting electrical power through concrete walls. An equation for the theoretical transmission efficiency that considers the copper and core losses was derived through equivalent circuit analysis. There is good agreement between the experimental and calculated values. The transmission efficiency was found to be strongly dependent on the shape of the magnet pole pieces. For a single flared shape, 165 W of power was transmitted over a distance of 100 mm through a concrete plate, representing a transmission efficiency of 78%. The efficiency dropped to approximately 67% for a concrete plate containing a steel frame.**

***Index Terms*—Concrete, magnetic resonance, robots, utility frequency, wireless power transmission (WPT).**

I. Introduction

THE ultimate goal of the present research is to develop a method for charging the batteries of robots operating in structures that humans cannot enter, such as areas contaminated by radioactivity, which is an issue that has become increasingly urgent in the wake of the Fukushima nuclear disaster. This would require energy being sent through thick concrete walls, possibly containing steel frames, so that workers could avoid contamination [1].

There are three possible methods of wireless power transmission (WPT): electromagnetic induction, magnetic resonance, and radio waves. Since resonant energy transfer was first developed by the WiTricity project [2], there has been a great deal of research carried out using this and other approaches [3]–[5]. Using magnetic resonance, Nagano Japan Radio Co. Ltd., succeeded in transmitting 1 kW of power over a distance of 300 mm at a high frequency of 13.56 MHz, with an efficiency of 88% [6]. The electromagnetic induction system developed by Pioneer Co. Ltd., used a 95 kHz power supply, and successfully transmitted 3 kW over a distance of 150 mm with an efficiency of 80% [7]. The WiTricity system is very simple, and the direction of research has progressed towards the design of devices such as inverters, and control techniques [8]–[10].

Electromagnetic waves are reflected and absorbed by concrete, by amounts that depend on the dielectric constant and conductivity of the material. Such effects are more pronounced in the case of reinforced concrete, which contains a steel frame, and it becomes difficult to transmit energy efficiently at megahertz frequencies [11]. Equipment that operates at frequencies above 10 kHz and power levels above 50 W is regulated by law in Japan. To avoid these constraints, a simple solution is to use a low frequency such as the common utility frequency.

Research into power transfer to electric vehicles using low-frequency electromagnetic induction was carried out by the Partners for Advanced Transit and Highways collaboration at the University of California over 30 years ago. Using a 400 Hz power supply, an efficiency of 60% was achieved over a distance of 100 mm [12]. However, since there has been little demand for such low-frequency systems, the techniques developed have not been substantially improved since that time, and after the development of the WiTricity system, there have been no attempts to use the commercial power grid frequency.

In the present study, the efficiency of resonant power transmission through concrete was investigated at the utility frequency of 60 Hz, using three different magnet pole piece configurations. The effect of a steel frame embedded in the concrete was also evaluated.

II. Experiment

The magnet pole pieces used in the present study were made from silicon steel plates with a thickness of 0.35 mm. They were cut using an electric discharge machine into the shapes shown in Table I. Three different shapes were considered, referred to P1 (rectangular), P2 (double flare), and P3 (single flare). The curvilinear regions followed a quadratic function. To define a suitably shaped magnet pole, we developed a simulator for magnetic field analysis based on the finite difference time domain (FDTD) method [13], [14]. Interlinkage and leakage of the magnetic field were expressed as 2-D images using the FDTD simulator.

At a frequency of 60 Hz, no saturation of the pole pieces was observed up to a flux density of 0.7 T. The coils were wound from single-strand enamel covered copper wire with a diameter of 2 mm. These prototypes were designed based on an assumed operating voltage and current of 200 V and 10 A, respectively. The same type of coil was used for the transmitter and receiver circuits. The weights shown in Table I are for a single coil,

Manuscript received February 3, 2014; revised April 9, 2014; accepted March 5, 2014. Date of publication May 22, 2014; date of current version October 15, 2014. Recommended for publication by Associate Editor C. T. Rim.

H. Ishida is with the Department of Electronics and Computer Engineering, Toyama National College of Technology, Toyama 933-0293, Japan (e-mail: ishida@nc-toyama.ac.jp).

H. Furukawa is with the Department of Electrical and Control Systems Engineering, Toyama National College of Technology, Toyama 933-0293, Japan (e-mail: function@nc-toyama.ac.jp).

Color version of one or more of the figures in this table are available online at http://ieeexplore.ieee.org.

Digital Object Identifier 10.1109/TPEL.2014.2322876

See http://www.ieee.org/publications_standards/publications/rights/index.html for more information.

TABLE I
SPECIFICATIONS OF THE FABRICATED DEVICES

	P1 (Rectangular type)	P2 (Double flare type)	P3 (Single flare type)
Schematic drawings	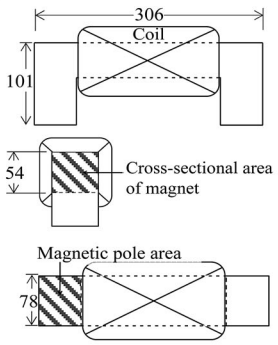	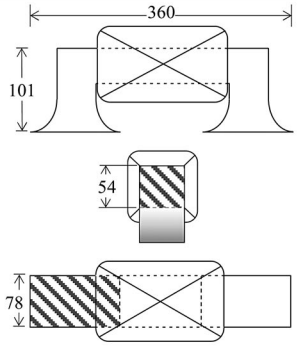	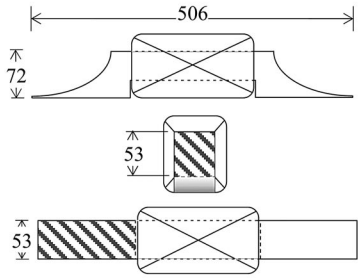
Weight	16.0 kg	16.8 kg	11.9 kg
Magnetic pole area	42 cm^2	84 cm^2	86 cm^2
Cross-sectional area of magnet	42 cm^2	42 cm^2	28 cm^2
Self-inductance of coils with magnet	Primary: 78.5 mH Secondary: 80.0 mH	Primary: 92.9 mH Secondary: 95.2 mH	Primary: 145.2 mH Secondary: 148.2 mH
Number of turns (layers)	375 turns (five-layers)	375 turns (five-layers)	450 turns (six-layers)
Winding resistance	Primary: 0.68 Ω Secondary: 0.69 Ω	Primary: 0.68 Ω Secondary: 0.68 Ω	Primary: 0.74 Ω Secondary: 0.78 Ω
Quality factor of coil at 60 Hz	Primary: 40.0 Secondary: 42.4	Primary: 45.3 Secondary: 46.7	Primary: 61.1 Secondary: 58.0

and do include the weight (1.15 kg) of the self-healing power condenser (N2 type, Panasonic Co. Ltd.).

The magnetic pole area for P2 was twice that for P1, and similar to that for P3. P3 had the smallest cross-sectional area of magnet in order to save weight. The coil used with P3 had a higher number of turns than the others, in order to compensate for the smaller cross-sectional area of magnet, the self-inductance in the absence of magnet pole piece is same as the other two coils. This allowed the effects of only the pole-piece shape to be examined.

We predicted the transmission power efficiency through analysis of the equivalent circuit of a 60-Hz WPT system. The parameters of the equivalent circuit used in the calculation (i.e., the transformer constants) were determined experimentally using an actual WPT device. The transformer constants were measured by using a frequency response analyzer (FRA5097, NF Co. Ltd.) and programmable ac power source (EC1000SA, NF Co. Ltd.). To determine the magnetic permeability, an inductor with a closed-loop core was needed, which we made in addition to three WPT devices.

Fig. 1 shows photographs of the experimental setup. Here, the transmitter and receiver are separated by acrylic plates so that an air gap exists between them. In the experiments simulating transmission through a concrete wall, a concrete plate with an area of 800 mm × 500 mm was placed in the air gap. This area was chosen to be sufficiently larger than the measured magnetic field spread. The thickness of the concrete plate was 50 or 100 mm. Its composition was cement, sand and gravel (25-mm particle size) with a weight ratio of 1:3:6. This composition is typical of concrete used in buildings. Concrete plates containing steel frames were also prepared.

III. CIRCUIT ANALYSIS

Fig. 2(a) shows a circuit diagram of the WPT system. For all of the results presented in this paper, the secondary condenser C_2 was connected in parallel with the load (PP mode). The configuration with C_2 connected in series (PS mode) can also be used. For the PP mode, the system acts as a constant current source, and for the PS mode as a constant potential source. Since the transmission efficiency in PS mode was found to be almost the same as that in PP mode, the experimental results for PS mode were omitted in this paper. When charging a lithium-ion battery, it is convenience to be able to shift between constant potential and constant current mode simply by changing a single condenser connection. The equivalent circuit for that in Fig. 2(a) is also simple, as shown in Fig. 2(b). Here, r_1 is the primary winding resistance, jx_1 is the primary leakage inductance, $-jx_{C1}$ is the primary capacitance, r_2 is the secondary winding resistance, jx_2 is the secondary leakage inductance, $-jx_{C2}$ is the secondary capacitance, r_c is the core loss, jx_L is the mutual inductance, and R_L is the load resistance.

When C_2 is connected, the following equation holds for a resonance frequency ω_0

$$x_{C2} = \frac{1}{\omega_0 C_2} = x_L + x_2. \tag{1}$$

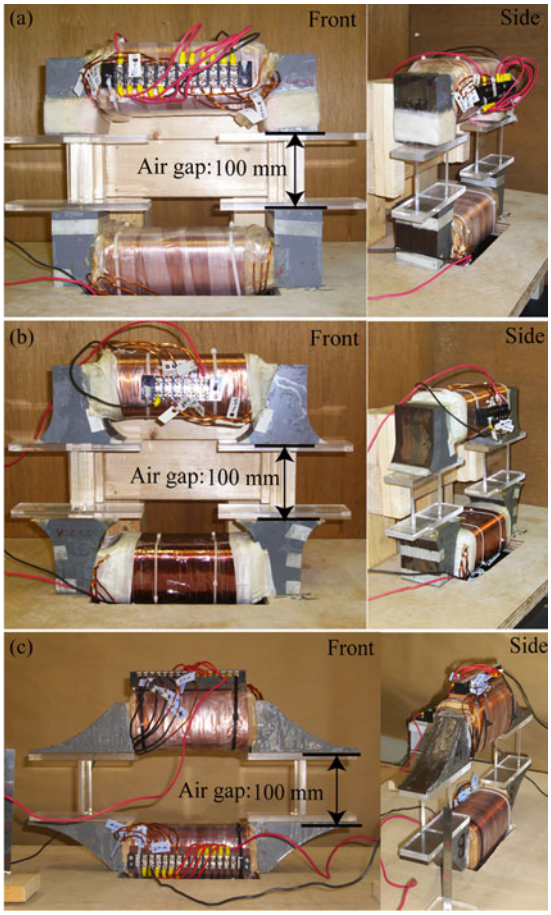

Fig. 1. Photographs of devices with pole pieces: (a) P1, (b) P2, and (c) P3.

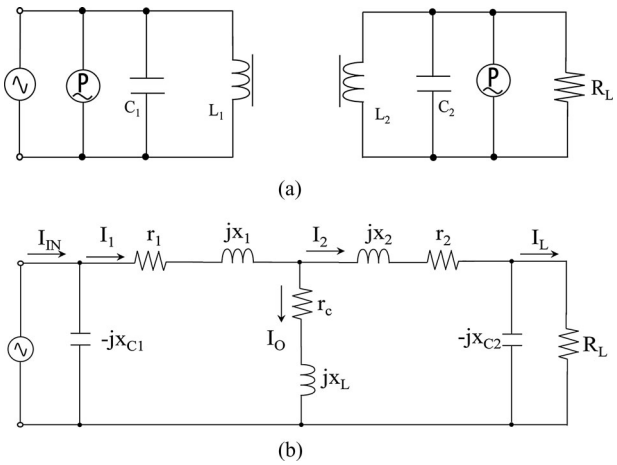

Fig. 2. WPT system: (a) circuit diagram and (b) equivalent circuit.

The overall impedance for the circuit in the absence of C_1 can be expressed using (2). Here, since the resistance components r_1, r_2, and r_c are sufficiently small compared to the reactance components, they were neglected

$$Z = \left(\frac{x_L}{x_L + x_2}\right)^2 R_L + j\left(\frac{x_L x_1 + x_1 x_2 + x_2 x_L}{x_L + x_2}\right). \quad (2)$$

When C_1 is connected, the condition for which the imaginary part of Z becomes zero is given by

$$x_{C1} = \frac{1}{\omega_0 C_1} = \frac{\left\{\left(\frac{x_L}{x_L + x_2}\right)^2 R_L\right\}^2}{\left(\frac{x_L x_1 + x_1 x_2 + x_2 x_L}{x_L + x_2}\right)} + \left(\frac{x_L x_1 + x_1 x_2 + x_2 x_L}{x_L + x_2}\right). \quad (3)$$

To derive an equation for the theoretical maximum transmission efficiency, we constructed an analysis method based on that of Tohi *et al.* in which the copper loss of the WPT is considered [15]. For the equivalent circuit shown in Fig. 2(b), the transmission efficiency considering the copper and core losses is as follows:

$$\eta = \frac{R_L I_L^2}{R_L I_L^2 + r_c I_0^2 + r_1 I_1^2 + r_2 I_2^2}. \quad (4)$$

When the turn ratio of the two coils is 1:1, the relationships between currents can be expressed as

$$\boldsymbol{I_1} = \alpha \boldsymbol{I_L},\ \alpha \equiv \frac{x_L + x_2}{x_L} \quad (5.1)$$

$$\boldsymbol{I_0} = \boldsymbol{I_1} - \boldsymbol{I_2} \quad (5.2)$$

$$|I_2| = |I_L|\sqrt{1 + \left(\frac{R_L}{x_{c2}}\right)^2} \quad (5.3)$$

$$|I_0|^2 = I_L^2\left[\alpha^2 + 1 + \left(\frac{R_L}{x_{c2}}\right)^2 - 2\alpha\sqrt{1 + \left(\frac{R_L}{x_{c2}}\right)^2}\cos\emptyset\right],$$

$$\cos\emptyset = \frac{x_{c2}}{\sqrt{R_L^2 + x_{c2}^2}}. \quad (5.4)$$

Substituting (5) into (4) yields, as shown (6), at the bottom of the page, where the value of $1/\alpha$ is very close to the coupling coefficient (k) when the inductances of the two coils are almost the same. The value of R_L for which the copper loss is minimized is given as follows [16]:

$$R_L = x_{c2}\sqrt{\alpha^2 \frac{r_1}{r_2} + 1}. \quad (7)$$

$$\eta = \frac{R_L}{R_L + r_1\alpha^2 + r_2\left\{1 + \left(\frac{R_L}{x_{c2}}\right)^2\right\} + r_c\left\{\alpha^2 + 1 + \left(\frac{R_L}{x_{c2}}\right)^2 - 2\alpha\sqrt{1 + \left(\frac{R_L}{x_{c2}}\right)^2}\cos\emptyset\right\}} \quad (6)$$

Thus, the maximum transmission efficiency considering the copper and core losses is

$$\eta_{\max} = \frac{1}{1+\frac{2r_2}{x_{c2}}\sqrt{\alpha^2\frac{r_1}{r_2}+1}+\frac{r_c\left\{\alpha^2\left(1+\frac{r_1}{r_2}\right)-2\alpha\sqrt{\alpha^2\frac{r_1}{r_2}+2}\cos\emptyset+2\right\}}{x_{c2}\sqrt{\alpha^2\frac{r_1}{r_2}+1}}}. \tag{8}$$

Here, k and the quality factors for the two coils (Q_1 and Q_2) Q_1 are defined as follows:

$$Q_1 = \frac{\omega_0 L_1}{r_1},\ Q_2 = \frac{\omega_0 L_2}{r_2},\ k = \frac{M}{\sqrt{L_1 L_2}},\ M = \frac{x_L}{x_L + x_2}L_2. \tag{9}$$

The maximum transmission efficiency of (8) can, thus, be rewritten as:

$$\eta_{\max} = \frac{1}{1+\frac{2r_2}{x_{c2}}\sqrt{\frac{1}{k^2}\frac{Q_2}{Q_1}+1}+\frac{r_c\left(\alpha^2+2+\frac{1}{k^2}\frac{Q_2}{Q_1}-2\alpha\sqrt{\frac{1}{k^2}\frac{Q_2}{Q_1}+2}\cos\emptyset\right)}{x_{c2}\sqrt{\frac{1}{k^2}\frac{Q_2}{Q_1}+1}}}. \tag{10}$$

Since (11) is true under any conditions, (10) can be approximated as shown by (12)

$$\frac{1}{k^2}\frac{Q_2}{Q_1} > 1 \tag{11}$$

$$\eta_{\max} \approx \frac{1}{1+\frac{2}{k\sqrt{Q_1 Q_2}}+\frac{2r_c(k+k^{-1}-1)}{r_2 Q_2}}. \tag{12}$$

Three conclusions can be derived from (12): 1) a large value of the product of k and Q yields high efficiency, 2) a large value of the product of r_2 and Q_2 (i.e., ωL_2) is also required for high efficiency, and 3) both copper and core losses increase with decreasing k (i.e., increasing transmission distance). It was not necessary to consider core loss for a high-frequency system without a magnetic core. Considering the core loss will be of particular importance for silicon steel cores.

IV. Results and Discussion

When the operating frequency is high, the Q factor is large, so a high efficiency can be achieved even when k is small [17], [18]. However, at low frequency, k must be larger since the Q factor is small. Thus, the shape of the magnet pole piece is very important at low frequencies. Fig. 3 shows the variation in k with transmission distance for the three different pole pieces. Here, the condensers for producing resonance were not connected. Since the magnetic pole area for P2 is twice that for P1, the magnetic reluctance was lower for P2, leading to larger k values. However, the highest k values are obtained for P3, even though this pole piece has the same area as P2 and P3.

We consider the FDTD simulation a useful method for the theoretical prediction of k. The problems encountered in this simulation were due to the very long wave length of 60 Hz (approx. 5000 km). Since the computation time depends on the ratio of wavelength to test-model size, an enormous time is required compared with that of the electromagnetic-field analysis of microwaves. Furthermore, computation should be continued until a steady state is reached. Simulation on the real scale is impossible at present. We carried out the simulation on a scale 10 000 times that of the actual test-model size. We were unable to decrease the enormous computation time required except by enlarging the scale. Even so, to obtain a 2-D image, our personal computer required 10 h (CPU-clock: 2.90 GHz). Thus, the computation time needed to obtain a 3-D image will be 23 000 h.

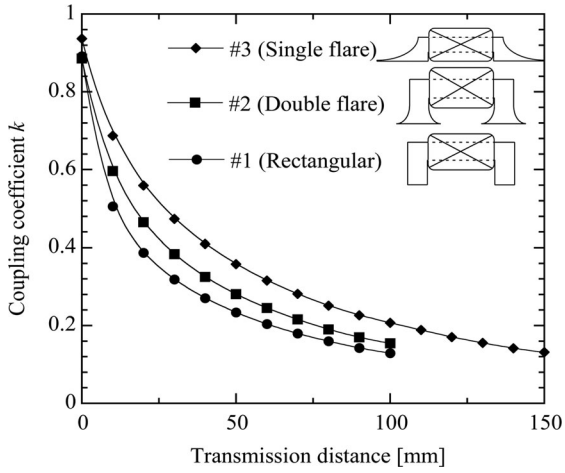

Fig. 3. Dependence of k on transmission distance.

Fig. 4 shows the simulation results of P1 and P3 for the transmission distance of 100 mm. The 2-D magnetic field is expressed as a contour graph of strength (H). We calculated H in the xy-plane only, assuming that there is no component in the depth (z) direction. The transmitter was placed on the upper side, and the receiver on the lower side. The virtual coils were wound similarly to those on actual devices. The two condensers used to produce resonance were not connected in the simulation, because the leakage inductances were compensated for by condensers. Fig. 4(a) and (b) were taken 4.25 periods after the power supply was turned ON, which supplied an alternating voltage of 200 V at 60 Hz. Loops I and II show the main routes of the interlinkage and leakage flux, respectively. There is no region of locally high H with P3 [see Fig. 4(b)]. The field is not high even at the tip of the magnet poles. This result suggests that abnormally high core loss does not occur. We found that a quadratic function allows weight of the device reduction. When it becomes possible to significantly reduce the calculation time, we will be able to estimate k for a 3-D magnetic field, and optimize its value by performing simulations with various magnet-pole shapes.

Fig. 5 shows the dependence of the transmission efficiency on the transmission distance for an input voltage of 200 V. The lines in the graph were calculated using the maximum efficiency given by (12). For the transmission distance of 50 mm, the parameters specified in Table II were used for the calculation,

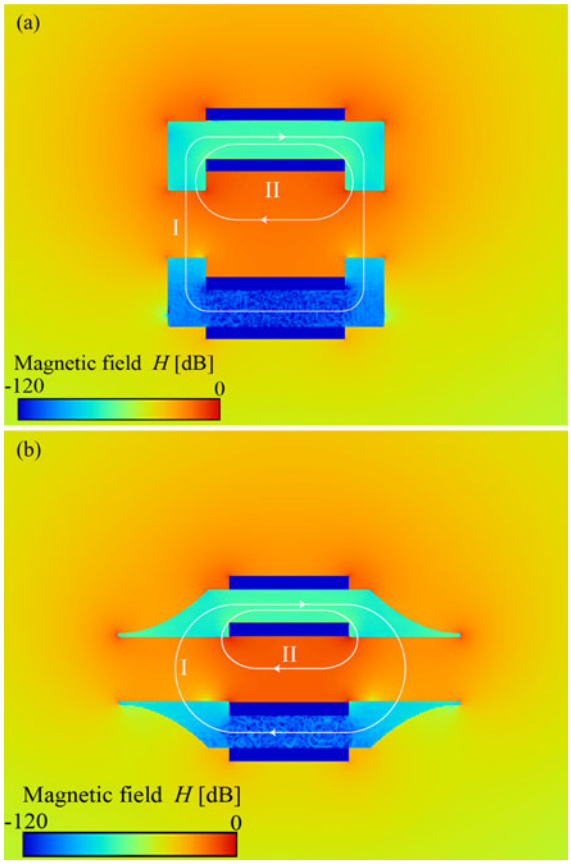

Fig. 4. Simulation results for a transmission distance of 100 mm: (a) P1 and (b) P3. Initial permeability of silicon steel was 2000, and winding for perfect conductance was assumed.

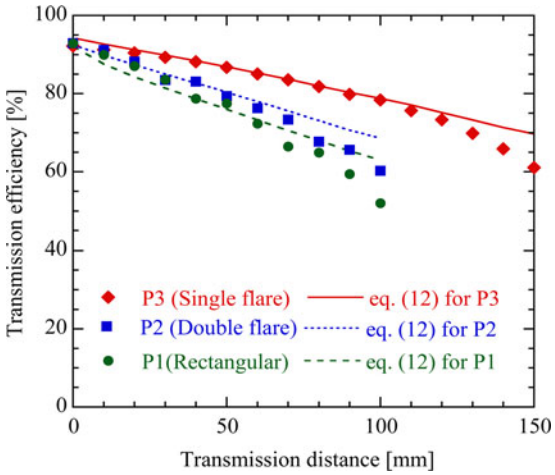

Fig. 5. Dependence of transmission efficiency on distance.

which are the experimentally obtained data. The calculated values of x_{c1}, x_{c2}, and R_L are given in parentheses in Table II. In Fig. 5, there is good agreement between the experimental and calculated values. However, effects other than copper and core loss are occurring for large transmission distances. As the transmission distance increases, the magnetic field surrounding

TABLE II
SPECIFIED PARAMETERS FOR THE TRANSMISSION DISTANCE OF 50 MM

	P1 (rectangular)	P2 (double flare)	P3 (single flare)
x_1 [Ω]	23.8	27.6	40.3
x_2 [Ω]	25.7	28.1	41.5
x_L [Ω]	7.83	11.0	23.1
r_c [Ω]	0.46	0.50	0.60
x_{c1} [Ω]	31.2 (31.9)	35.4 (40.0)	53.1 (64.1)
x_{c2} [Ω]	33.2 (33.5)	35.4 (39.1)	57.4 (64.6)
R_L [Ω]	146.5 (146.3)	159.2 (144.7)	173.6 (187.4)

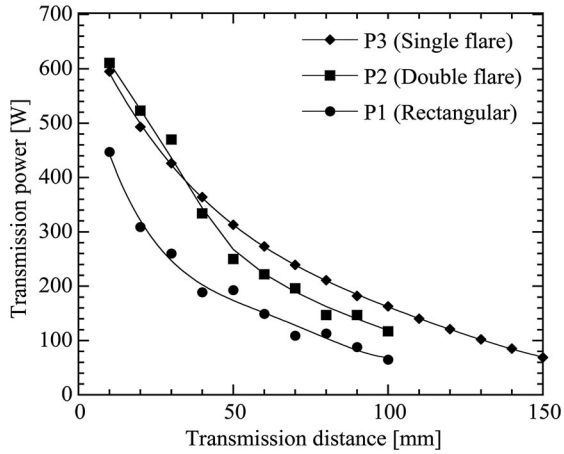

Fig. 6. Dependence of transmission power on distance.

the magnetic pole expands into free space. Therefore, stray load loss is thought to occur. Although we do not understand this phenomenon perfectly, to the best of our knowledge, there have been no reports on devices displaying a higher efficiency than P3 with the utility frequency of 60 Hz; that said our device is yet to be optimized.

Fig. 6 shows the variation in the transmitted power with distance. Fitting curves were drawn by the fourth-order polynomial least square. For short transmission distances, the power simply depends on the magnetic pole area, so that similar results are obtained for P2 and P3. However, for distances above 50 mm, a clear effect of the pole-piece shape is observed, with higher transmitted power being achieved by P3.

A feature of the present study was the choice to use 60 Hz. The variation in the maximum efficiency with different power supply frequencies is discussed in this section. The permeability (μ) and r_c of the magnet pole piece strongly depend on the power supply frequency. Fig. 7 shows the frequency dependence of μ and r_c. Here, μ was measured under the same magnetic flux density (0.59 T) with a transmission distance of 50 mm for P3. Frequencies over 550 Hz could not be measured due to the limit of the power supply unit. The frequency dependences of both parameters were consistent with previous findings [19], [20]. We calculated the power supply frequency dependence of the maximum efficiency and power loss using (12) and the experimental results shown in Fig. 7. The results shown in Fig. 8 were obtained with a transmission distance of 50 mm for P3.

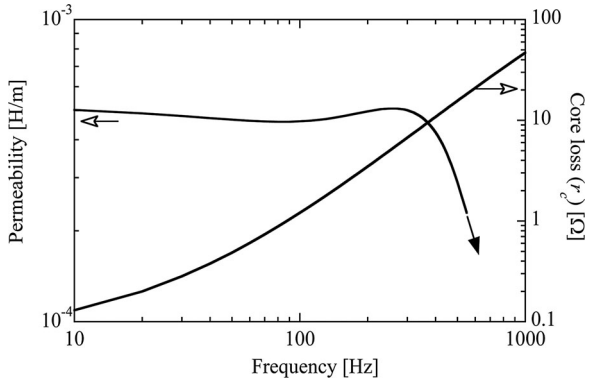

Fig. 7. Frequency dependence of μ and r_c for P3.

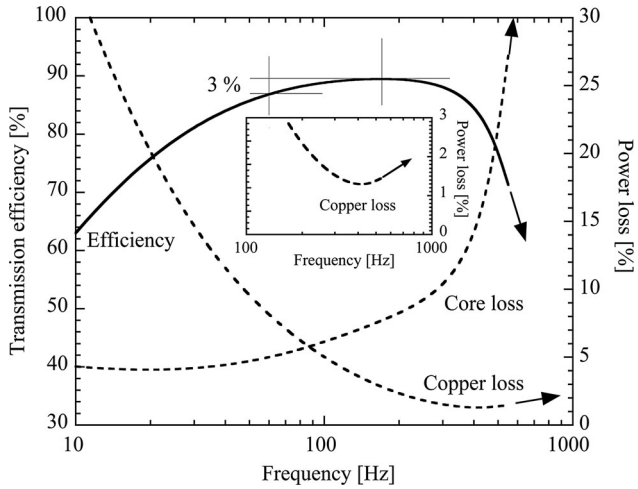

Fig. 8. Dependence on power supply frequency of the maximum efficiency and power loss.

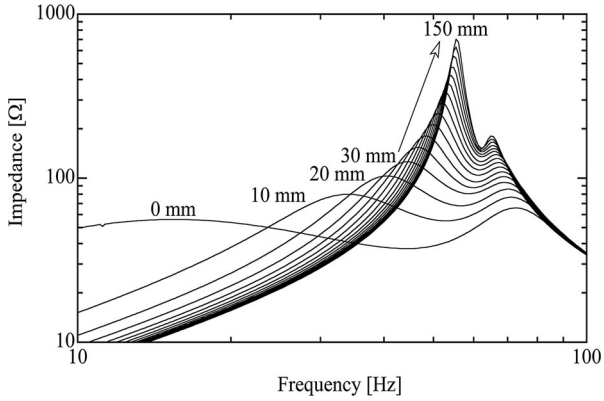

Fig. 9. Impedance characteristics for P3.

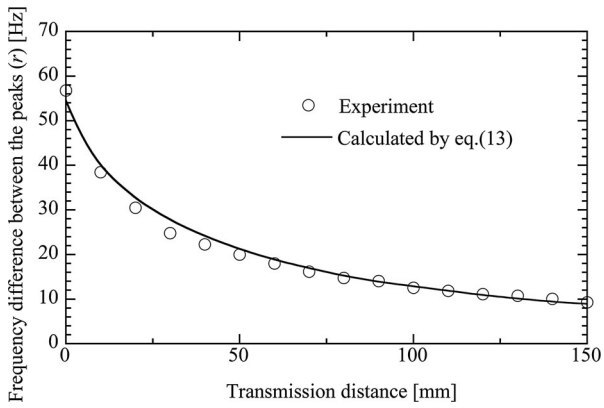

Fig. 10. Dependence of r on transmission distance.

The core loss suddenly increases for frequencies over 300 Hz. The inset shows an expanded view of the copper loss curve. The copper loss slowly increases for frequencies over 400 Hz. As a result, the curve of maximum efficiency is parabolic in shape. The maximum efficiency of 90% was reached at 170 Hz. With 60 Hz an efficiency of 87% was attained, which is consistent with the experimental results (see Fig. 5). We have to consider the power loss associated with the conversion to 170 Hz from the utility frequency. For example, the power efficiency with a high-performance ac–dc converter is around 98% [21], and that with a dc–ac inverter is around 98% [22], [23]. AC–AC direct conversion can be achieved with an efficiency of 95% [24]. Thus, the total power loss will not be less than 4% for the conversion of 60 to 170 Hz. For this reason, we concluded that directly transmitting 60 Hz is the optimal solution.

A magnet pole piece made from a ferrite such as Mn-Zn, with a litz wire winding, will exhibit high performance under a power supply frequency of 10 kHz. Tohi *et al.* calculated the maximum efficiency at 10 kHz with a transmission distance of 30 mm to be 93% [15]. However, experimental values will be less than this, because this value does not include the core loss. With the 60-Hz system, 90% was obtained for a transmission distance of 30 mm (see Fig. 5). We consider the 60-Hz system to be advantageous considering the power loss associated with the conversion from the utility frequency to 10 kHz.

Fig. 9 shows the impedance characteristics of P3 for different transmission distances. Two peaks can be seen, and the dip between them occurs at the resonance frequency. The frequency difference (r) between the peaks is seen to decrease with increasing transmission distance. These results indicate that although the frequency is very low, energy transfer between the transmitter coil and the receiver coil occurs by coupling of the evanescent tails of the two resonant circuits. For the case of evanescent tail coupling, r can be expressed by

$$\mathrm{r} \propto \sqrt{\Delta f^2 + k^2}. \tag{13}$$

Here, Δf is the difference between the resonance frequencies of the two resonant circuits. Although Δf should be zero for perfect resonance, in reality it was 0.08 Hz. The dependence of r on the transmission distance is plotted in Fig. 10. The solid line is the calculated value, and it is seen to agree well with the experimental results.

For the results shown in Fig. 9, the values of the two condensers were set to optimize at transmission distance of 50 mm. Therefore, the resonance frequency increased with transmission distance. However, the change in resonance frequency is

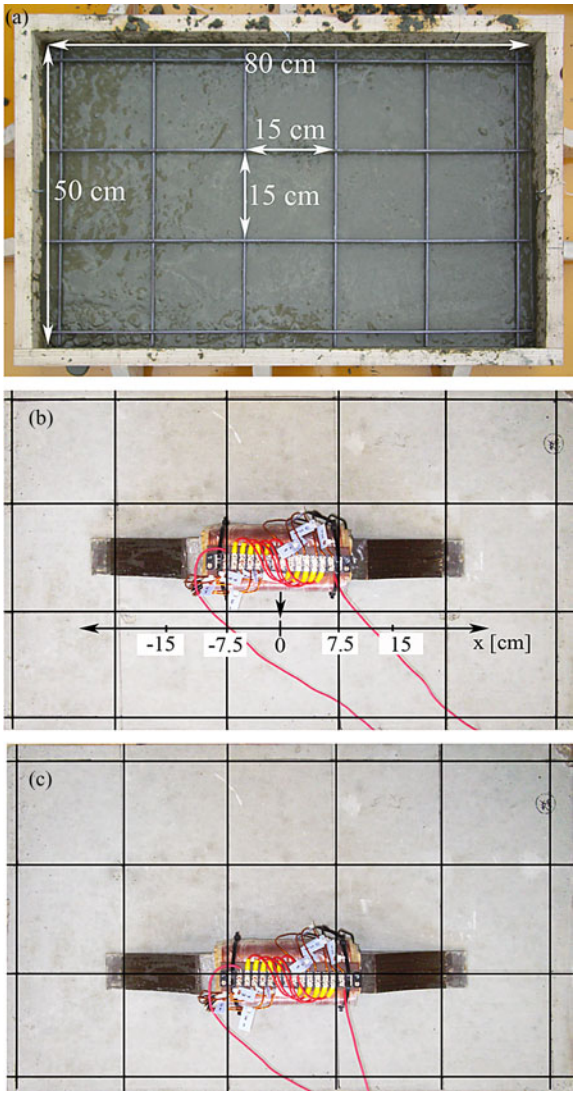

Fig. 11. Photographs of steel-embedded concrete: (a) layout of steel frame, (b) device position A, and (c) device position B.

very small from 50 to 100 mm. For practical applications of this system, changes in the transmission distance must be taken into consideration. Since the Q factor is smaller at low frequencies, the impedance is less dependent on the transmission distance. Accordingly, this system acts as a stabilized power supply and does not require frequency control. In contrast, since the Q factor is very large at high frequencies, the impedance is very sensitive to transmission distance, and needs to be adjusted if the transmission distance changes [10], [25].

The change in performance was next investigated when a concrete plate with a thickness of 50 or 100 mm was inserted into the air gap. Concrete plates containing steel frames were also used. As shown in Fig. 11(a), the frames were constructed using steel rods with a diameter of 5 mm, which were arranged in a square lattice with separations of 150 mm. The steel frames were buried at the center of the concrete plates. Since it was expected that the transmission performance would depend on the relative position of the device and the steel frame, the device

TABLE III
EXPERIMENTAL RESULTS FOR CONCRETE FRAMES

		50-mm thick	100-mm thick
Air	Power	313 W	163 W
	Efficiency	86.7%	78.3%
Concrete	Power	314 W	165 W
	Efficiency	86.5%	78.3%
Reinforced concrete (position A)	Power	266 W	139 W
	Efficiency	75.4%	67.1%
Reinforced concrete (position B)	Power	264 W	139 W
	Efficiency	75.2%	67.1%

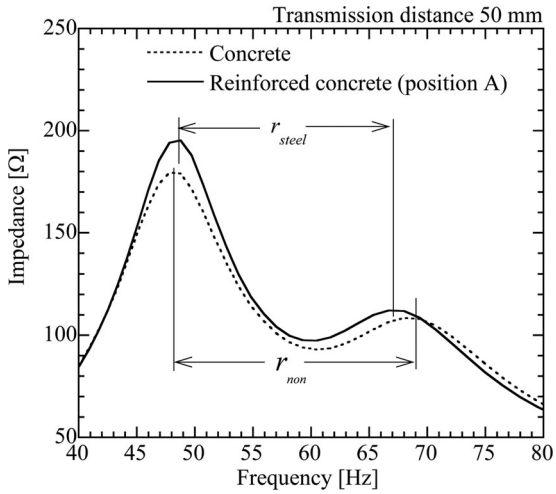

Fig. 12. Impedance characteristics for concrete plates with or without steel frame.

was tested at two different vertical positions A and B, as shown in Fig. 11(b) and (c), respectively. The experimental results are shown in Table III. Since concrete interacts with a magnetic field in a similar manner to air, there was little difference in the experimental results when concrete alone was inserted. For an air or concrete thickness of 50 and 100 mm, the transmission efficiency was about 86% and 78%, respectively. This dropped to 75% and 67%, respectively, when a steel plate was present in the concrete. In both cases, this represents a decrease of 11%. There was little difference between the results for positions A and B.

It is thought that the steel frame suppressed the coupling between the two coils. Fig. 12 shows a comparison of the impedance characteristics for concrete plates with and without steel frames. The presence of the steel frame causes the spacing between the two peaks to decrease, indicating a reduction in k. The reduction of k estimated by (13) was approximately 0.05. The power loss resulting from a reduction of 0.05 would be 2.0% as estimated by (12). Equation (12) describes only the power loss generated inside the device. Eddy currents are generated in steel frames by an alternating magnetic field, resulting in approximately 9% of the input power being consumed by Joule heating.

Fig. 13 shows the simulation for the case in which the steel frames are set in concrete 50 mm thick. We found that the

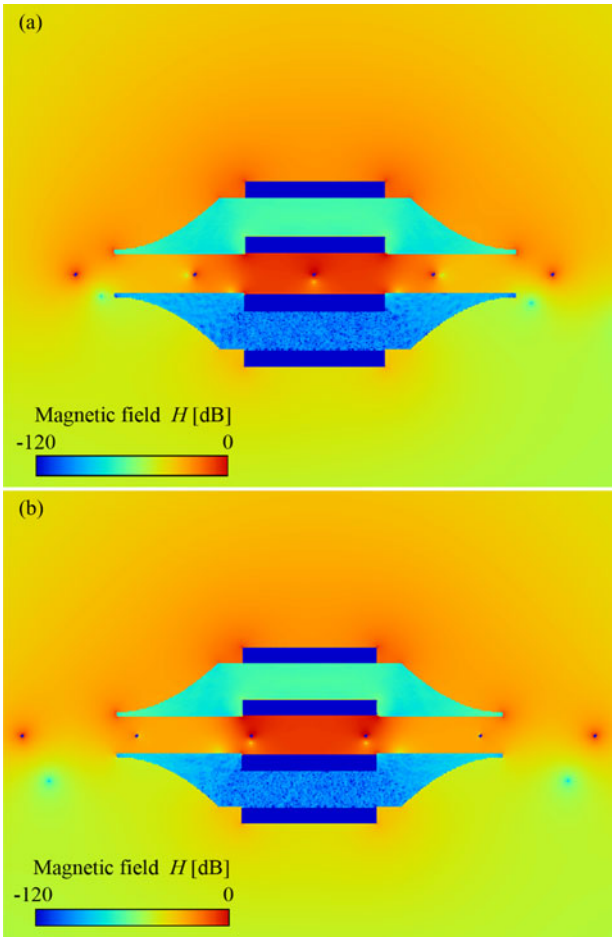

Fig. 13. Simulations of steel frames set in concrete 50 mm thick. Plots (a) and (b) show different positions of the device relative to the steel frame. The relative permittivity of concrete is 9 [26], and the steel rod was assumed to be a perfect conductor.

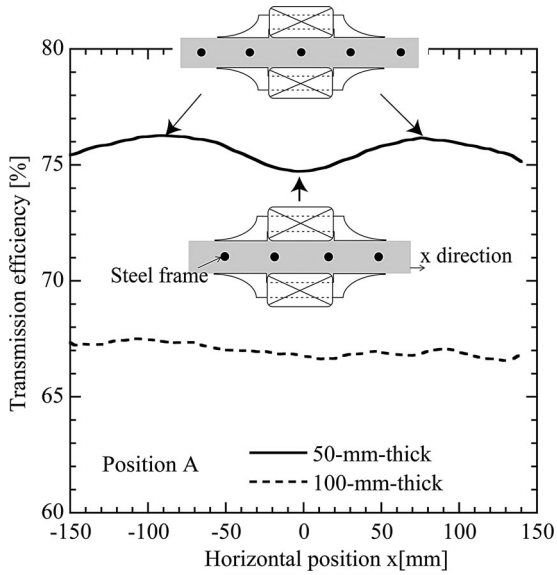

Fig. 14. Variation in transmission efficiency with horizontal position. The insets show the position of the device relative to the steel frame at a maximum and minimum.

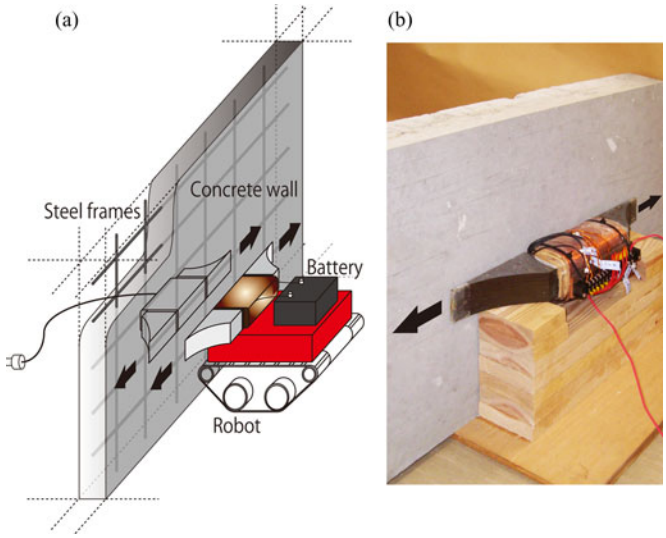

Fig. 15. Power transmission through concrete wall: (a) schematic of working robot with wireless charging system, and (b) experimental setup.

magnetic field was concentrated around the steel frame. The case without a steel frame is shown in Fig. 16(a). The leakage of the magnetic field was increased by the steel frames. Steel rods in the leakage flux (i.e., Loop II) were the primary cause of reduced efficiency; thus, the efficiency will vary depending on the number of such steel rods. The efficiency of the setup shown in Fig. 13(a) may be better than that in Fig. 13(b). This hypothesis was proven experimentally and is discussed in the next section.

The two coils were moved horizontally relative to the reference position shown in Fig. 11(b). Fig. 14 shows the variation in transmission efficiency with horizontal position (x) for concrete thicknesses of 50 and 100 mm. The largest variation of about 3% was found for the 50-mm-thick concrete plate. The figure also indicates the position of the coils relative to the steel frame at positions of maximum and minimum efficiency. For the 100-mm-thick concrete plate, the variation was not founded. When the two coils moved in the vertical direction, the efficiency changed only very slightly even with the 50-mm-thick concrete.

When considering practical applications of such a device, it is also necessary to investigate the effect of lateral displacement of the two coils. As illustrated in Fig. 15, if the device was being used to recharge a robot, although little vertical displacement would be expected, lateral displacement would occur because the robot would not necessarily stop at the same position each time. We carried out FDTD simulations to investigate the effects of lateral displacement. Fig. 16(a) shows the simulation for no displacement. Fig. 16(b) shows a displacement of 13 cm. The main route of the leakage flux changed in Fig. 16(b). In the receiver, we confirmed that the magnetic field became weak around the right-hand pole. It is suggested that the interlinking magnetic field became weak as a result.

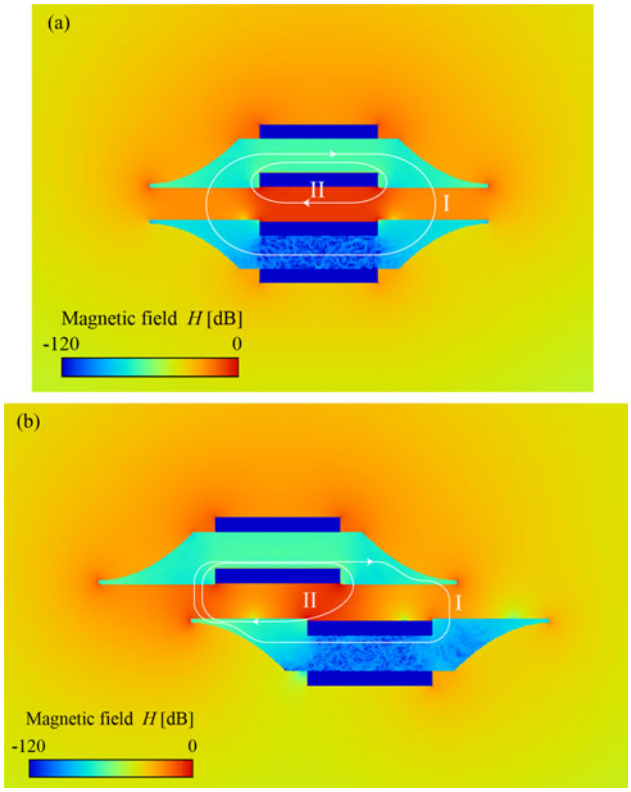

Fig. 16. Simulation of lateral displacement for P3: (a) no displacement and (b) 13-cm displacement.

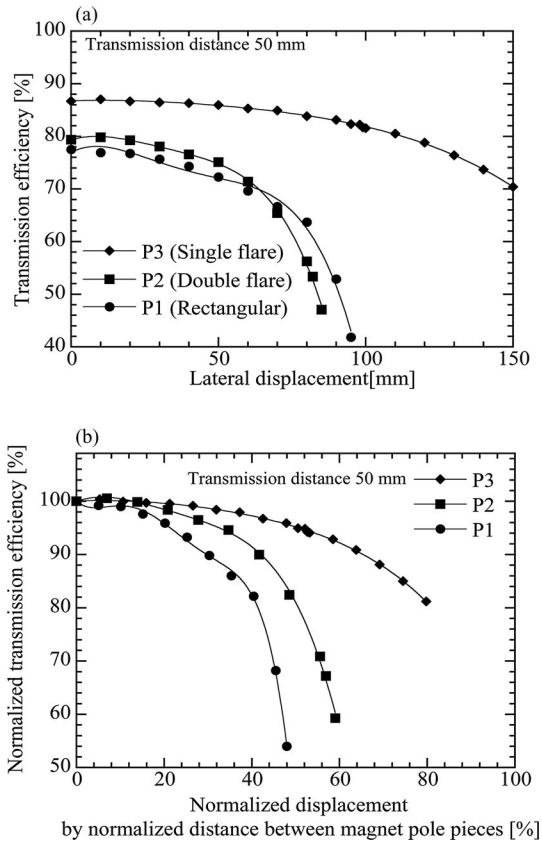

Fig. 17. Dependence of transmission efficiency on lateral displacement: (a) absolute values and (b) normalized values.

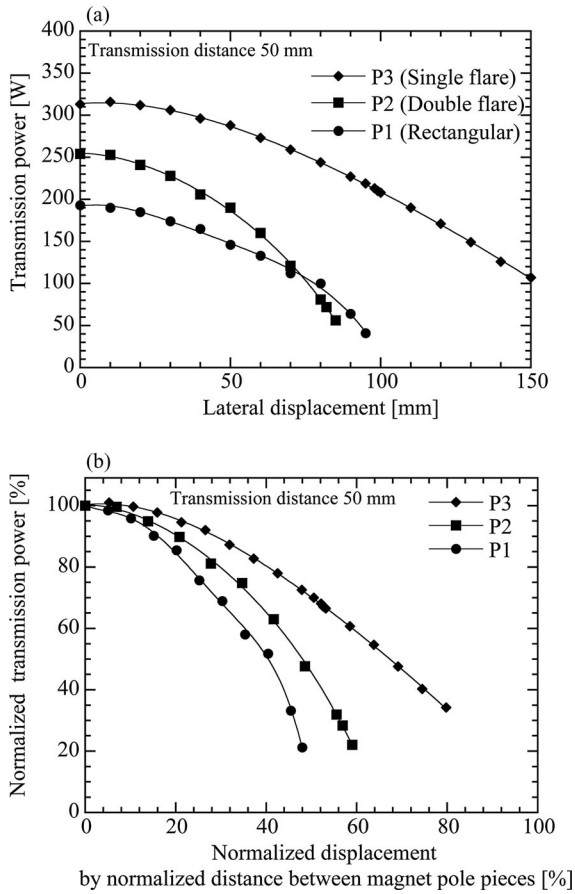

Fig. 18. Dependence of transmission power on lateral displacement: (a) absolute values and (b) normalized values.

Figs. 17(a) and 18(a) show the variations in transmission efficiency and transmitted power, respectively, with lateral displacement for the three pole pieces. This experiment was carried out for a concrete plate with a thickness of 50 mm with no steel frame. Fitting curves were drawn by the fourth-order polynomial least square. From the figures, it can be seen that the best results were obtained for P3 and the worst for P2. Similar results were obtained for the thicker concrete plate. The reason for this is thought to be that, since the distance between the magnet pole pieces is shortest for P2, a magnetic flux loop is formed in the primary coil as the lateral displacement increases. The distances between the magnet pole pieces were 198, 144, and 188 mm in P1, P2, and P3, respectively. To appropriately compare the three devices, the x-axis values were normalized by the distance between the magnet pole pieces. In addition the y-axes were normalized by the efficiency and power in the case of no displacement. The normalized graphs are shown in Figs. 17(b) and 18(b). If the distance between the magnet pole pieces of P2 is increased, P2 will benefit from lateral displacement. Regardless, P3 is the best of the three devices. We think that the variations in the characteristics resulting from lateral displacement are explained well by the values of k. When a 3-D simulator is realized, prediction of these characteristics will be possible.

V. Conclusion

Obtaining a large Q factor is difficult at low frequencies, which is the reason why low-frequency approaches have not been used until now. However, when silicon steel is used as the magnetic core, the transmission efficiency will be maximized at the very low frequency of 170 Hz. To the best of our knowledge, this is the first time this result has been reported. We took the total transmission efficiency into consideration, and concluded that the utility frequency of 60 Hz is the optimal choice. Our system can be directly connected to a wall socket.

WPT using evanescent tail coupling between two resonant circuits was investigated. Although the principle involved is similar to that used by WiTricity, the frequency used is the common utility frequency. Higher frequency systems do not need magnetic cores; therefore, the weight and transmission distance are superior to those of our system. However, using the utility frequency, it was found that power could be transferred efficiently, even through a concrete plate. When a steel frame was embedded in the concrete, degradation did occur, and mitigating this effect is a subject for further work. A working system of this type is expected to find applications in disaster-struck areas such as the nuclear power plant in Fukushima Prefecture, Japan.

Acknowledgment

The authors would like to thank Dr. T. Miyake (Toyama Prefectural University) for development of the FDTD simulation.

References

[1] K. Nagatani, S. Kiribayashi, Y. Okada, K. Otake, K. Yoshida, S. Tadokoro, T. Nishimura, T. Yoshida, E. Koyanagi, M. Fukushima, and S. Kawatsuma, "Emergency response to the nuclear accident at the Fukushima daiichi nuclear power plants using mobile rescue robots," *J. Field Robot.*, vol. 30, pp. 44–63, Jan. 2013.

[2] A. Kurs, A. Karalis, R. Moffatt, J. D. Joannopoulos, P. Fisher, and M. Soljacic, "Wireless power transfer via strongly coupled magnetic resonances," *Science*, vol. 317, pp. 83–86, Jul. 2007.

[3] B. L. Cannon, J. F. Hoburg, D. D. Stancil, and S. C. Goldstein, "Magnetic resonant coupling as a potential means for wireless power transfer to multiple small receivers," *IEEE Trans. Power Electron.*, vol. 24, no. 7, pp. 1819–1826, Jul. 2009.

[4] A. Kurs, R. Moffatt, and M. Soljacic, "Simultaneous mid-range power transfer to multiple devices," *Appl. Phys. Lett.*, vol. 96, no. 044102, Jan. 2010, DOI: 10.1063/1.3284651.

[5] A. S. Y. Poon, S. O' Driscoll, and T. H. Meng, "Optimal frequency for wireless power transmission into dispersive tissue," *IEEE Trans. Antennas Propag.*, vol. 58, no. 5, pp. 1739–1750, May 2010.

[6] Y. Yokoi, A. Taniya, M. Horiuchi, and S. Kobayashi, "Development of kW class wireless power transmission system for EV using magnetic resonant method," in *Proc. Int. Elect. Vehicle Technol. Conf.*, May 2011, no. 20117267, pp. 1–6.

[7] E. Urushibata, "General outline of wireless charging system for EV/PHV as well as its development trend and the future," IEICE Tech. Rep., no. WPT 2012–24, pp. 23–26, Nov. 2012. (in Japanese)

[8] W. Fu, B. Zhang, and D. Qiu, "Study on frequency tracking wireless power transfer system by resonant coupling," in *Proc. IEEE Int. Power Electron. Motion Control Conf.*, May 2009, pp. 2658–2663.

[9] K. Kusaka and J. Itoh, "Reduction of reflected power loss in an AC–DC converter for wireless power transfer systems," *IEEJ J. Ind. Appl.*, vol. 2, no. 4, pp. 195–203, Mar. 2013.

[10] Z. N. Low, R. Chinga, R. Tseng, and I. Lin, "Design and test of a high power high efficiency loosely coupled planar wireless power transfer system," *IEEE Trans. Ind. Electron.*, vol. 56, no. 5, pp. 1801–1812, May 2009.

[11] D. Pena, R. Feick, H. Hristov, and W. Grote, "Measurement and modeling of propagation losses in brick and concrete walls for the 900-MHz band," *IEEE Trans. Antennas Propag.*, vol. 51, no. 1, pp. 31–39, Jan. 2003.

[12] C. E. Zell and J. G. Bolger, "Development of an engineering prototype of a roadway powered electric transit vehicle system," in *Proc. IEEE Veh. Technol. Conf.*, May 1982, vol. 32, pp. 435–438.

[13] C. Sijoy and S. Chaturvedi, "Calculation of accurate resistance and inductance for complex magnetic coils using the finite-difference time-domain technique for electromagnetics," *IEEE Trans. Plasma Sci.*, vol. 36, no. 1, pp. 70–79, Feb. 2008.

[14] X. Yu, S. Sandhu, S. Beiker, R. Sassoon, and S. Fan, "Wireless energy transfer with the presence of metallic planes," *Appl. Phys. Lett.*, vol. 99, no. 214102, Nov. 2011, DOI: 10.1063/1.3663576.

[15] T. Tohi, Y. Kaneko, and S. Abe, "Maximum efficiency of contactless power transfer systems using k and Q," *IEEJ Trans. Ind. Appl.*, vol. 132, no. 1, pp. 123–124, Jan. 2012.

[16] T. Imura, "Study on maximum air-gap and efficiency of magnetic resonant coupling for wireless power transfer using equivalent circuit," in *Proc. IEEE Int. Symp. Ind. Electron.*, Jul. 2010, pp. 3664–3669.

[17] A. Sample, D. Meyer, and J. Smith, "Analysis, experimental results, and range adaptation of magnetically coupled resonators for wireless power transfer," *IEEE Trans. Ind. Electron.*, vol. 58, no. 2, pp. 544–554, Feb. 2011.

[18] C.-J. Chen, T.-H. Chu, C.-L. Lin, and Z.-C. Jou, "A study of loosely coupled coils for wireless power transfer," *IEEE Trans. Circuits Syst. II, Exp. Briefs*, vol. 57, no. 7, pp. 536–540, Jul. 2010.

[19] F. Fiorillo and A. Novikov, "An improved approach to power losses in magnetic laminations under nonsinusoidal induction waveform," *IEEE Trans. Magn.*, vol. 26, no. 5, pp. 2904–2910, Sep. 1990.

[20] W. Hutchinson and J. Swift, "Anisotropy in some soft magnetic materials," *Texture*, vol. 1, pp. 117–123, Jun. 1972.

[21] G. Gong, M. L. Heldwein, U. Drofenik, J. Minibock, K. Mino, and J. W. Kolar, "Comparative evaluation of three-phase high-power-factor AC–DC converter concepts for application in future more electric aircraft," *IEEE Trans. Ind. Electron.*, vol. 53, no. 3, pp. 727–737, Jun. 2005.

[22] S. Kjaer, J. Pedersen, and F. Blaabjerg, "A review of single-phase grid-connected inverters for photovoltaic modules," *IEEE Trans. Ind. Appl.*, vol. 41, no. 5, pp. 1292–1306, Sep. 2005.

[23] T. Kerekes, R. Teodorescu, P. Rodriguez, G. Vazquez, and E. Aldabas, "A new high-efficiency single-phase transformerless PV inverter topology," *IEEE Trans. Ind. Electron.*, vol. 58, no. 1, pp. 184–191, Jan. 2011.

[24] J. Itoh, T. Iida, and A. Odaka, "Realization of high efficiency AC link converter system based on AC/AC direct conversion techniques with RB-IGBT," in *Proc. IEEE 32nd Annu. Conf. Ind. Electron.*, Jul. 2006, pp. 1703–1708.

[25] P. Si, A. P. Hu, S. Malpas, and D. Budgett, "A frequency control method for regulating wireless power to implantable devices," *IEEE Trans. Biomed. Circuits Syst.*, vol. 2, no. 1, pp. 22–29, Mar. 2008.

[26] A. Muqaibel, A. Safaai-Jazi, A. Bayram, A. M. Attiya, and S. M. Riad, "Ultrawideband through-the-wall propagation," *IEE Proc. Microw. Antennas Propag.*, vol. 152, pp. 581–588, Dec. 2005.

Hiroki Ishida received the Ph.D. degree in electrical engineering from Nagaoka University of Technology, Niigata, Japan, in 2004.

He joined the Toyama National College of Technology in 2005, and has been an Associate Professor there since 2010. He is engaged in research on superconducting Josephson devices. His current research interests include development of laser Doppler velocimetry for noninvasive *in-vivo* imaging of blood vessels.

Dr. Ishida is a member of the Institute of Electrical Engineers of Japan and the Japan Society of Applied Physics.

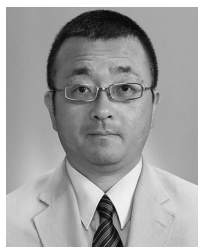

Hiroto Furukawa received the B.S. and M.S. degrees in electrical engineering from Tokyo Denki University, Japan, in 1987 and 1989, respectively.

He joined the Toyama National College of Technology in 1991, and has been an Associate Professor there since 2003. He has been engaged in propagation characteristics of microwave in concrete blocks and its application for nondestructive diagnostics.

Mr. Furukawa is a member of the Institute of Electrical Engineers of Japan and the Institute of Electronics, Information and Communication Engineers.